

# LEARNING COLOR SPACE ADAPTATION FROM SYNTHETIC TO REAL IMAGES OF CIRRUS CLOUDS

Qing Lyu, Xiang Chen

Zhejiang University

**Abstract.** Training on synthetic data is becoming popular in vision due to the convenient acquisition of accurate pixel-level labels. But the domain gap between synthetic and real images significantly degrades the performance of the trained model. We propose a color space adaptation method to bridge the gap. A set of closed-form operations are adopted to make color space adjustments while preserving the labels. We embed these operations into a two-stage learning approach, and demonstrate the adaptation efficacy on the semantic segmentation task of cirrus clouds.

## 1 INTRODUCTION

Recent success in supervised learning typically requires a large amount of labeled training data. Since manual labeling is often time-consuming and error-prone, training on synthetic images has become increasingly popular in vision tasks, such as object detection[1,2,3,4], viewpoints estimation[5,6,7,8], and semantic segmentation[9]. For example, photorealistic rendering on 3D models is able to provide an accurate pixel-level annotation for each object in the scene, which eliminates the labeling cost for image segmentation learning. Under such circumstances, several synthetic datasets like Virtual KITTI [3] and SYNTHIA [10] have been generated for training and evaluating vision models.

However, the inherent domain gap leads to a performance degradation when the model trained on the synthetic dataset is directly used on the real-world images. Such kind of gaps may result from many reasons, *e.g.* differences in geometric details, textures, backgrounds, and lightings. Although it's tempting to design a versatile domain transfer model to bridge the gaps at once, we argue that dividing the factors provides a better opportunity for optimizing each individual subtask. Among these factors, the difference in color space plays a key role. In some sense, synthetic images generated by physically based renderer are pure raw data, while real images are noisy data post-processed either by digital cameras or photography softwares.

In this paper, we propose a color space adaptation framework to transfer a synthetic dataset to a given target of real images. Specifically, we adopt a set of basic operations for color space adjustments. The reason is twofold. First, these closed-form operations merely affect color representation, without incurring any perceptual difference and label damage. As a result, we leverage such properties

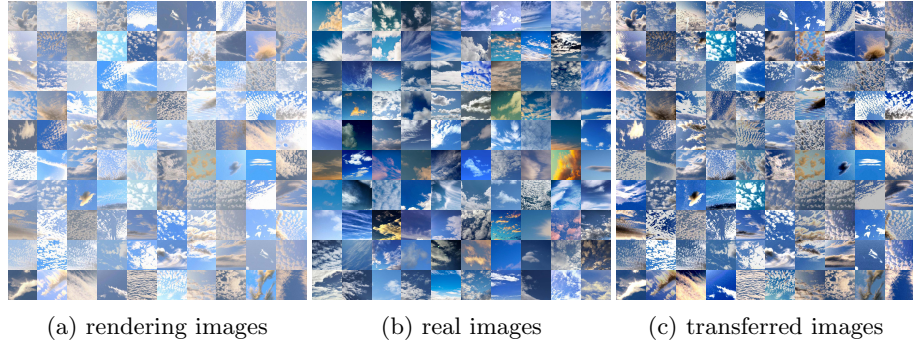


Fig. 1: COLOR SPACE ADAPTATION. Compared with the original photorealistic rendering images (a), the transferred images (c) after the color space adaption are visually more consistent with the real images (b). Please refer to the supplementary material for complete results.

to generate sufficient adversarial examples for pre-training an effective classifier that is only sensitive to colors, but not to shapes and textures. Second, we are able to train a generative network to transfer the synthetic dataset to the real images, by taking the classifier as a loss function of the color representation differences between the two domains. The basic operations are also embedded in the generative network, using the intermediate outputs as their color adjustment parameters.

We quantitatively evaluate the efficacy of the proposed color space adaptation framework on a synthetic cirrus clouds dataset (see Fig. 1). We build this new dataset mainly for challenging cloud image segmentation. Our experiments show that the transferred dataset has significantly improved the segmentation performance compared with the original one.

## 2 RELATED WORK

**Synthetic-to-Real Domain Adaptation** Visual domain adaptation once focused on the transformation of latent distributions in feature space [1,11]. With the remarkably generative capability of GANs, recent methods begin to convert synthetic images in pixel-level. Bousmalis *et al.* [12] combine a content-similarity loss with GANs to generate contexts around synthetic subjects mimicking the target domain. CyCADA [13] combines cycle-consistency constraints with GANs to transfer the synthetic images at both pixel-level and feature-level. This line of work usually requires a dedicated loss formulation to balance the preservation of images contents. We avoid the loss design by using exactly content-preserving operations to generate color space variants of real images for training the classifier. RenderGAN [14] inserts a parameterized 3D model with a cascade of image augmentations into the GANs to imitate the tag images rendering process. We

focus on the color space adaptation of a synthetic dataset of diverse shapes for semantic segmentation, rather than rendering a template model from scratch for tag recognition.

**Color Transformation** Learning color transformations, *e.g.* enhancement, stylization and colorization, from given image examples is a challenging problem [15]. There have been some efforts in training DNN or CNN to learn from a set of paired images before and after transformation [16,17]. Recently, unpaired data are instead learned to either search for good exemplars to stylize the input image [18], or generate a retouching sequence that is meaningful to human [19]. We also learn from unpaired data, but a discriminator network is trained to guide the synthetic dataset adaptation to promote vision tasks.

**Image Segmentation** As a fundamental task in computer vision, pixel-level labeling ushers in a new development in semantic segmentation [20,21] and instance segmentation [22]. Synthetic data have also been generated for training segmentation models [9]. We adapt the synthetic data towards real-world images to bridge their domain gap in color space, and consider this as an effective way to improve segmentation performance.

### 3 METHOD

The color space adaptation is a learning approach that is trained on unpaired images. Given a real image dataset  $X_r$  without labels, and a synthetic image dataset  $X_s$  with segmentation labels  $Y_s$ , we expect to learn a function  $\mathbf{g}_{s \rightarrow r}$  to adapt  $X_s$  towards  $X_r$ , while preserving  $Y_s$ . This amounts to an optimization problem

$$\min_{\mathbf{g}_{s \rightarrow r}} \mathbb{E}_{x_s \sim X_s} \log [1 - \mathbf{d}(\mathbf{g}_{s \rightarrow r}(x_s), X_r)], \quad (1)$$

where  $\mathbf{g}_{s \rightarrow r}$  is label-preserving, and  $\mathbf{d}$  is a function measuring how close an input image is to the dataset  $X_r$  in their color space representations.

To embody the discriminative function  $\mathbf{d}$ , we choose to sample sufficient variants of  $X_r$  in color space as  $X_{rv}$ , and consequently train a classifier to distinguish between  $X_r$  and the adversarial dataset  $X_{rv}$ . Therefore, we adopt the composition of a set of basic image processing operators, *i.e.*  $\mathbf{ops} := \mathbf{op}_b \circ \mathbf{op}_s \circ \mathbf{op}_c$ , to randomly adjust the brightness, saturation and contrast of images in  $X_r$ . These low-level operators ensure that the learned classifier is only effective in distinguishing the color representations of the images, but insensitive to their high-level perceptual difference. We define the discriminative function as

$$\mathbf{d}(\star, X_r) := \arg \min_{\mathbf{D}} \mathbb{E}_{x_r \sim X_r} \log [\mathbf{D}(x_r)] + \mathbb{E}_{x_{rv} \sim X_{rv}} \log [1 - \mathbf{D}(x_{rv})], \quad (2)$$

where  $X_{rv} = \text{randn}(X_r, \mathbf{ops})$ , whose details are given later.

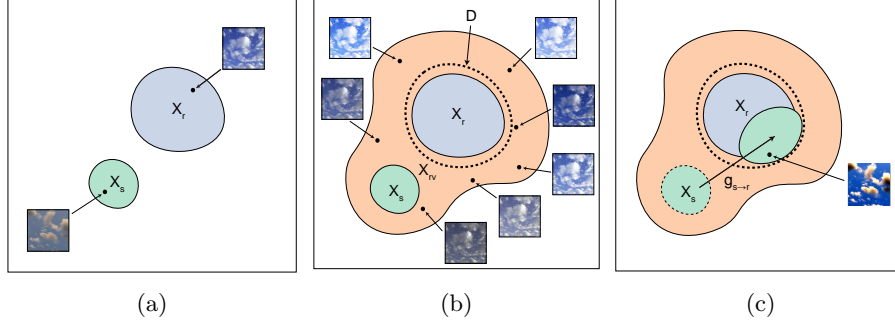


Fig. 2: METHOD. The synthetic images  $X_s$  and real images represent distinct subsets  $X_r$  in the color space (a). Color adjustment operations are used to generate random variants  $X_{rv}$  of the real images  $X_r$ . A discriminator  $D$  is trained to classify  $X_{rv}$  and  $X_r$  well in color space (b). Next, the generator is trained to adapt the synthetic images  $X_s$  under the guidance of the pre-trained discriminator  $D$ . The transferred synthetic images  $g_{s \rightarrow r}(X_s)$  after the adaptation is much more close to the real images  $X_r$  in the color space (c).

In order to ensure that  $g_{s \rightarrow r}$  does not destroy the segmentation labels, we define it as a color space adaptation function  $g_{s \rightarrow r}(\star) := \text{ops}(\star, G(\star))$ , where  $G$  maps the input image to the color adjustment parameters applied on it.

Accordingly, our training process has two stages. i) following Eqn. 2, we learn the discriminator  $D$  by pre-training on  $X_r$  and  $X_{rv}$  (see Fig. 2b); ii) following Eqn. 1, we learn the generator  $G$ , under the guidance of the pre-trained  $D$  (see Fig. 2c).

Note that we do not exactly follow the standard GANs to train  $D$  by classifying the transferred synthetic images  $g_{s \rightarrow r}(X_s)$  and the real images  $X_r$ . Because this simply results in a discriminator that is color-insensitive due to the dominance of perceptual content differences (*e.g.* shapes, textures) between  $X_s$  and  $X_r$ . Instead, we prevent  $D$  from observing the synthetic data  $X_s$  during training. We pre-train  $D$  to classify  $X_{rv}$  and  $X_r$  merely from their differences in color representation, which consequently ensures that  $G$  (instructed by  $D$ ) is able to adapt the color space information of  $X_s$  correctly, and also means that we need not repeat the above two-stages training process alternatively.

**Adversarial Data** The adversarial data are color space variants of real images generated by the function `randn`. This function first samples the color adjustment parameters according to a non-standard normal distribution,  $\alpha \sim \mathcal{N}(\mu, \sigma)$ . Then it applies color adjustment operations to obtain  $X_{rv} = \{\text{ops}(x, \alpha) \text{ for } x \in X_r\}$ . We compute the mean and standard deviation of  $\mathcal{N}$  as

$$\mu = 0, \quad \int_{-1}^1 \frac{1}{\sqrt{2\pi\sigma^2}} e^{-\frac{(\alpha-\mu)^2}{2\sigma^2}} = p, \quad (3)$$

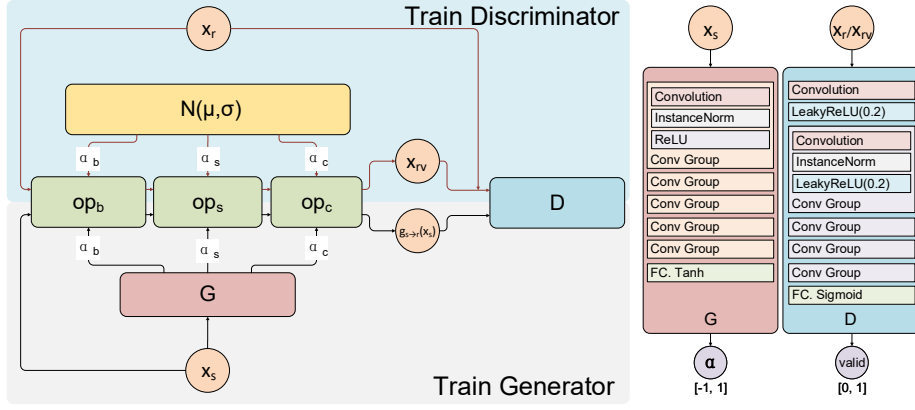


Fig. 3: PIPELINE AND ARCHITECTURE. On the left, we show the pipeline of our system. The top panel contains the modules for training the discriminator, while the bottom one contains the modules for training the generator. The module of color adjustment operations is shared between the two stages. It takes in Gaussian random samples as parameters to generate adversarial data for training the discriminator, and takes in the generator output as parameters to generate adapted synthetic images for training the generator. On the right, we show the architectures of the generator network and discriminator network. See the main text for details.

where  $p$  is the probability that  $\alpha$  falls in the range  $[-1, 1]$ . We set  $p = 0.99$  to ensure that  $\alpha$  is in the usual range of color adjustment in most cases. Please see the Appendix A for the full details of ops.

**Discriminator** We design the network structure of the discriminator D (see the rightmost part of Fig. 3) by following the guidelines of DCGANs [23]. Specifically, we use strided convolutions to replace pooling layers and choose Leaky ReLUs (with slope coefficient 0.2) as the activation function. We also use instance normalization instead of batch normalization. The convolution group, including a convolution layer, an instance normalization layer and a leaky ReLU layer, are repeated four times, and at last a fully connected layer is connected with a sigmoid function as the output. In the first training stage (Fig. 2b), the adversarial data  $X_{rv}$  and real images  $X_r$  are fed into this network to train the parameters of D.

**Synthetic Data** We construct a cirrus cloud dataset of 11,654 synthetic images. First, we computationally generate 624 3D volume data with heterogeneous grid densities, through fluid simulation and image-based reconstruction. Then, we use physically based renderer Mitsuba [24] to generate photorealistic images, as well as the segmentation labels, from those volume data of cirrus clouds. We randomly

sampled the parameters of the volume rendering, *e.g.* scene lighting, reflections, lens focal length, and camera viewpoint, in order to extend the coverage range. The generated synthetic images all have  $512 \times 340$  resolution.<sup>1</sup>

**Generator** The color adjustment operations **ops** are embedded into  $\mathbf{g}_{s \rightarrow r}$ , by taking the output of the generator  $\mathbf{G}$  as the adjustment parameters  $\alpha$  (see Fig. 3). In some sense, this mimics the post-processing steps taken by photographers in the real world to retouch raw images. Specifically, the generator is composed of three components with the same network structure, *i.e.*  $\mathbf{G} = \{\mathbf{G}_b, \mathbf{G}_s, \mathbf{G}_c\}$ . Each component takes an input image and produces an adjustment parameter for an operator in **ops** respectively,  $\alpha = \{\alpha_b = \mathbf{G}_b(x), \alpha_s = \mathbf{G}_s(x), \alpha_c = \mathbf{G}_c(x)\}$ . Finally, the **ops** together with the produced  $\alpha$  are applied on the input image to generate an adapted one.

Again, we design the network structure of the generator  $\mathbf{G}$  (see the right part of Fig. 3) by following the guidelines of DCGANs [23]. The convolution group, including a convolution layer, an instance normalization layer and a ReLU layer, are repeated five times, and at last a fully connected layer is connected with a tanh function as the output. In the second training stage (Fig. 2c), the synthetic images  $X_s$  are fed into the network  $\mathbf{G}$  to train its parameters, by maximizing the score of the adapted images  $\mathbf{g}_{s \rightarrow r}(X_s)$  obtained on the pre-trained discriminator  $\mathbf{D}$  (fixed in this stage).

## 4 EXPERIMENTS

### 4.1 Implementation Details

All our implementations are based on the Keras library [25] with the TensorFlow [26] backend. A desktop machine with Ubuntu 16.04 and a Geforce 1080Ti GPU is used for training the neural networks.

**Adaptation Training** For all the experiments, we choose 24 as the batch size. The input images are zero-centered and rescaled to  $[-1, 1]$ . The network weights are initialized with He initialization [27]. We adopt the Adam optimizer [28], and train all the networks from scratch with  $lr = 1e-3$  and  $\beta_1 = 0.5$ . First, the discriminator is trained for 30K iterations. Then the generator is trained for 30K iterations with the pre-trained discriminator frozen. The loss change during the training process is shown in Fig. 4a. When training  $\mathbf{D}$ , we get a loss value around 0.32 for training data and 0.25 for test data. When training  $\mathbf{G}$ , we get a loss value around 1.39 for training data and 1.83 for test data.

Partial results of the synthetic images before and after color space adaptation are shown in Fig. 1. Visually, the adapted images are much more similar to the color style of real images. The SWD metric [29] between the synthetic images

<sup>1</sup> We will release the cirrus clouds dataset soon, including all the volume data, rendering settings and rendering results.

and the real images has reduced about 55% after the adaptation. More results can be found in the supplementary material.

**Segmentation Training** The FCN-8s architecture [20] is used to perform the semantic segmentation task. We fine-tune the network with the VGG-16 model, and adopt the SGD optimizer with the learning rate of  $1e-5$  and the momentum of 0.9. Mean squared error is used as the loss function. We iterate the training process for 250 epochs and achieve a stable training accuracy around 0.9. The accuracy change during the training process is shown in Fig. 4b.

## 4.2 Evaluation

**Baseline and Comparison** We quantitatively evaluate the color space adaptation method through the performance of semantic segmentation tasks. Specifically, we prepare four datasets for training the segmentation network:

- *Synthetic images*. 7,969 synthetic images with automatic generated segmentation labels through physically based rendering (see description in Section 3).
- *Adapted synthetic images*. The synthetic images after the color space adaptation, with the original segmentation labels preserved.
- *Augmented synthetic images*. 21,252 augmented images by random sampling the parameters to apply color adjustment operations on the original synthetic images.
- *Real images*. 273 real images with manually annotated segmentation labels. Because of the complex boundaries of cirrus clouds, manual labeling is extremely time-consuming. We just annotate sufficient cirrus images for fine-

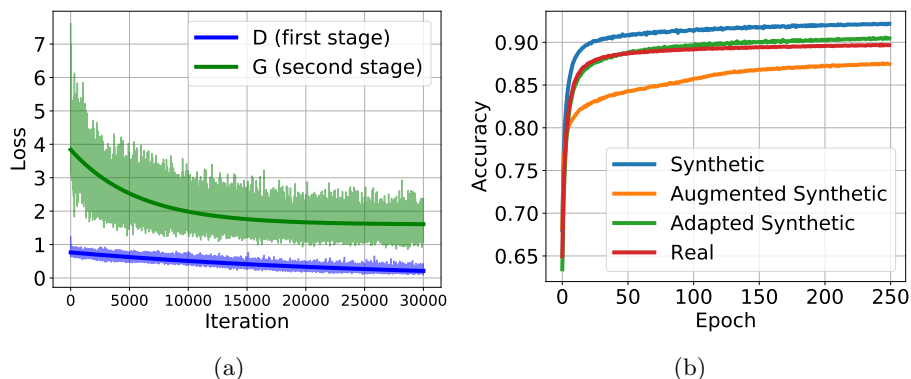


Fig. 4: TRAINING PROCESS. (a) Losses of the discriminator and the generator, during the first and second stage of the color space adaptation training. (b) The FCN accuracies during the semantic segmentation training.

tuning the FCNs. Note that this dataset has no overlap with the real images for color space adaptation.

Finally, we annotate another 154 real images as the unique test dataset to evaluate the segmentation performance of the FCNs trained on the above four datasets.

Table 1 shows the evaluation results. Compared with the original synthetic images, the randomly augmented synthetic images has only less than 2% relative improvement. On the other hand, using the adapted synthetic images as training data has improved the segmentation performance from 0.68 to 0.75 (about 10% relative improvement), which proves the efficacy of our color space adaptation method. The performance of adapted images is very close to the performance of the real images. This demonstrates that it's promising to replace the real images with synthetic images to eliminate the manual labeling efforts, at least partially. In fact, using the combined dataset with the adapted images and the real images together, we obtain a segmentation performance of 0.7765, which is higher than merely using the real images.

**Ablations** In Eqn. 3, we could have different choices of  $p$ , *i.e.* the probability of the adjustment parameter  $\alpha$  in the range  $[-1, 1]$ . We test the segmentation performance by setting  $p$  to 0.9, 0.99 and 0.999 during the adaptation, respectively. Table 2 shows that the change of  $p$  brings slight variations to the mean IoU scores. In practice, we've found that  $p = 0.99$  is a reasonably good choice to all the experiments.

Table 1: mean IoU for all datasets.

Training Dataset	mean IoU (test)
synthetic images	0.6829
augmented synthetic images	0.6996
adapted synthetic images	<b>0.7488</b>
real images	<b>0.7668</b>

Table 2: mean IoU for different adaptation options.

idx	$p$ (in Eqn.3)			D (second stage)		mean IoU
	0.9	0.99	0.999	fixed	non-fixed	
0	✓			✓		0.7359
1		✓		✓		<b>0.7488</b>
2			✓	✓		0.7458
3		✓			✓	0.6247
4			✓		✓	0.6753



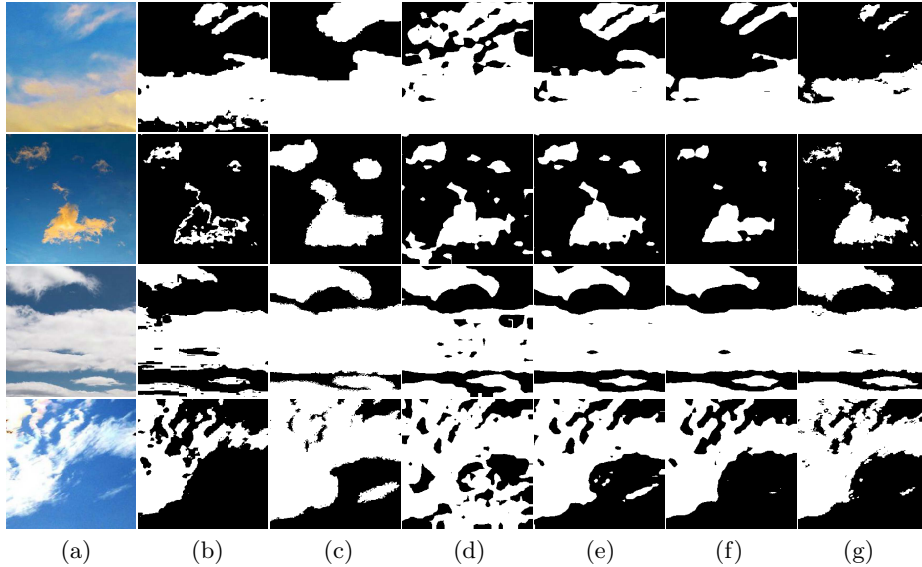


Fig. 5: SEGMENTATION RESULTS. (a) The original images. (b) The chromatic segmentation [30]. (c) The paint selection segmentation [31]. (d) The segmentation trained on the original synthetic images. (e) The segmentation trained on the synthetic images after color space adaptation. (f) The segmentation trained on the manual labeled real images. (g) The ground truth segmentation labels.

In the second training stage of the adaptation, we fix the discriminator  $D$  to train the generator  $G$ . We could also relax this condition to put  $D$  into backprop. However, Table 2 shows that by doing this the segmentation performance quickly degrades, to be even worse than using non-adapted images. As discussed in Section 3, a possible reason is that once the discriminator starts to observe the synthetic images, the perceptual information like shapes and textures could gradually dominate the classification.

### 4.3 Applications

We show some segmentation results in Fig. 5. The interactive segmentation methods (Fig. 5b and 5c) are often tedious and time-consuming to yield a reasonable annotation result. The segmentation results by using the original synthetic images for training have obvious artifacts (Fig. 5d). On the other hand, using the adapted synthetic images for training significantly improves the segmentation accuracy (Fig. 5e), whose results are visually quite similar with that of using manual labelled images for training (Fig. 5f) and the ground truth (Fig. 5g). Finally, we are able to do some further applications based on the segmentation results.

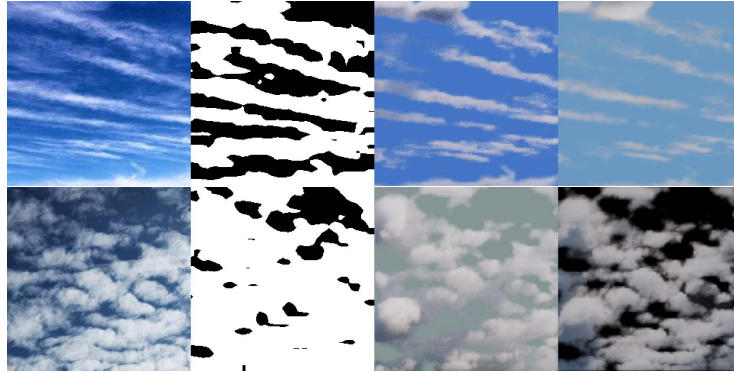


Fig. 6: FURTHER APPLICATIONS. The single image based 3D volume data reconstruction of cirrus clouds.

**3D Reconstruction** By leveraging the trained segmentation network, we generate the segmentation label as input to reconstruct the 3D volume data from a cirrus cloud image [30], and re-render it under new lighting conditions to produce novel images (Fig. 6).

**Matting and Composition** We execute image matting [32] based on a tri-map computed from the inflated segmentation label, to first separate the cirrus cloud foreground from the source image (Fig. 7 left), and then paste it onto other target images (Fig. 7 mid) to recompose novel cirrus clouds images (Fig. 7 right).

## 5 CONCLUSIONS

We have introduced a color space adaptation method for bridging the gap between synthetic and real images. The adaptation method is a two-stage learning approach. A sequence of label-preserving operations is adopted in both two stages to make variants in the color space. We demonstrate that training on the adapted synthetic cirrus cloud images has significantly improved the semantic segmentation performance compared with training on the original ones.

Our framework is extensible, other kinds of operations can be introduced to enable more complex color adjustment effects, *e.g.* the spatially variant curves adjustment. This capability is essential to adapt dataset like Virtual KITTI [3] (see supplementary material), due to the complicated factors in its gap to the real world. Moreover, although our rendering images are photorealistic, their details are still not comparable to high-resolution real images, given the limited computational resources in practice. Therefore, it is promising to learn a generative network that is able to add perceptual details into the synthetic images but without destroying their labelings, and combine it into the adaptation framework.

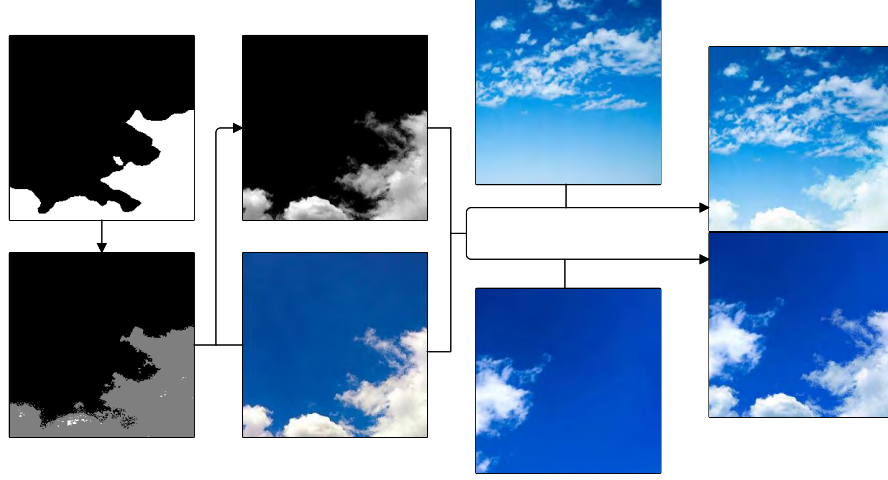


Fig. 7: FURTHER APPLICATIONS. The cirrus clouds image matting and composition.

## References

1. Sun, B., Saenko, K.: From virtual to reality: Fast adaptation of virtual object detectors to real domains. In: BMVC. Volume 1. (2014) 3
2. Massa, F., Russell, B.C., Aubry, M.: Deep exemplar 2d-3d detection by adapting from real to rendered views. In: Proceedings of the IEEE Conference on Computer Vision and Pattern Recognition. (2016) 6024–6033
3. Gaidon, A., Wang, Q., Cabon, Y., Vig, E.: Virtual worlds as proxy for multi-object tracking analysis. In: Proceedings of the IEEE conference on computer vision and pattern recognition. (2016) 4340–4349
4. Tobin, J., Fong, R., Ray, A., Schneider, J., Zaremba, W., Abbeel, P.: Domain randomization for transferring deep neural networks from simulation to the real world. In: Intelligent Robots and Systems (IROS), 2017 IEEE/RSJ International Conference on, IEEE (2017) 23–30
5. Liebelt, J., Schmid, C.: Multi-view object class detection with a 3d geometric model. In: CVPR 2010-23rd IEEE Conference on Computer Vision & Pattern Recognition, IEEE Computer Society (2010) 1688–1695
6. Stark, M., Goesele, M., Schiele, B.: Back to the future: Learning shape models from 3d cad data. In: Bmvc. Volume 2., Citeseer (2010) 5
7. Su, H., Qi, C.R., Li, Y., Guibas, L.J.: Render for cnn: Viewpoint estimation in images using cnns trained with rendered 3d model views. In: Proceedings of the IEEE International Conference on Computer Vision. (2015) 2686–2694
8. Grabner, A., Roth, P.M., Lepetit, V.: 3d pose estimation and 3d model retrieval for objects in the wild. In: Proceedings of the IEEE Conference on Computer Vision and Pattern Recognition. (2018) 3022–3031

9. Richter, S.R., Vineet, V., Roth, S., Koltun, V.: Playing for data: Ground truth from computer games. In: European Conference on Computer Vision, Springer (2016) 102–118
10. Ros, G., Sellart, L., Materzynska, J., Vazquez, D., Lopez, A.M.: The synthia dataset: A large collection of synthetic images for semantic segmentation of urban scenes. In: Proceedings of the IEEE conference on computer vision and pattern recognition. (2016) 3234–3243
11. Long, M., Cao, Y., Wang, J., Jordan, M.I.: Learning transferable features with deep adaptation networks. arXiv preprint arXiv:1502.02791 (2015)
12. Bousmalis, K., Silberman, N., Dohan, D., Erhan, D., Krishnan, D.: Unsupervised pixel-level domain adaptation with generative adversarial networks. In: The IEEE Conference on Computer Vision and Pattern Recognition (CVPR). (2017)
13. Hoffman, J., Tzeng, E., Park, T., Zhu, J.Y., Isola, P., Saenko, K., Efros, A.A., Darrell, T.: Cycada: Cycle-consistent adversarial domain adaptation. arXiv preprint arXiv:1711.03213 (2017)
14. Sixt, L., Wild, B., Landgraf, T.: Rendergan: Generating realistic labeled data. *Frontiers in Robotics and AI* **5** (2018) 66
15. Wang, B., Yu, Y., Xu, Y.Q.: Example-based image color and tone style enhancement. *ACM Transactions on Graphics (TOG)* **30** (2011) 64
16. Limmer, M., Lensch, H.P.: Infrared colorization using deep convolutional neural networks. In: Machine Learning and Applications (ICMLA), 2016 15th IEEE International Conference on, IEEE (2016) 61–68
17. Yan, Z., Zhang, H., Wang, B., Paris, S., Yu, Y.: Automatic photo adjustment using deep neural networks. *ACM Transactions on Graphics (TOG)* **35** (2016) 11
18. Lee, J.Y., Sunkavalli, K., Lin, Z., Shen, X., So Kweon, I.: Automatic content-aware color and tone stylization. In: Proceedings of the IEEE Conference on Computer Vision and Pattern Recognition. (2016) 2470–2478
19. Hu, Y., He, H., Xu, C., Wang, B., Lin, S.: Exposure: A white-box photo post-processing framework. *ACM Transactions on Graphics (TOG)* **37** (2018) 26
20. Long, J., Shelhamer, E., Darrell, T.: Fully convolutional networks for semantic segmentation. In: Proceedings of the IEEE conference on computer vision and pattern recognition. (2015) 3431–3440
21. Chen, L.C., Papandreou, G., Kokkinos, I., Murphy, K., Yuille, A.L.: Deeplab: Semantic image segmentation with deep convolutional nets, atrous convolution, and fully connected crfs. *IEEE transactions on pattern analysis and machine intelligence* **40** (2018) 834–848
22. He, K., Gkioxari, G., Dollár, P., Girshick, R.: Mask r-cnn. In: Computer Vision (ICCV), 2017 IEEE International Conference on, IEEE (2017) 2980–2988
23. Radford, A., Metz, L., Chintala, S.: Unsupervised representation learning with deep convolutional generative adversarial networks. arXiv preprint arXiv:1511.06434 (2015)
24. Jakob, W.: Mitsuba renderer (2010) <http://www.mitsuba-renderer.org>.
25. Chollet, F., et al.: Keras. <https://keras.io> (2015)
26. Abadi, M., Barham, P., Chen, J., Chen, Z., Davis, A., Dean, J., Devin, M., Ghemawat, S., Irving, G., Isard, M., et al.: Tensorflow: a system for large-scale machine learning. In: OSDI. Volume 16. (2016) 265–283
27. He, K., Zhang, X., Ren, S., Sun, J.: Delving deep into rectifiers: Surpassing human-level performance on imagenet classification. In: Proceedings of the IEEE international conference on computer vision. (2015) 1026–1034
28. Kingma, D.P., Ba, J.: Adam: A method for stochastic optimization. arXiv preprint arXiv:1412.6980 (2014)

29. Bonneel, N., Rabin, J., Peyré, G., Pfister, H.: Sliced and radon wasserstein barycenters of measures. *Journal of Mathematical Imaging and Vision* **51** (2015) 22–45
30. Dobashi, Y., Shinzo, Y., Yamamoto, T.: Modeling of clouds from a single photograph. In: *Computer Graphics Forum*. Volume 29., Wiley Online Library (2010) 2083–2090
31. Liu, J., Sun, J., Shum, H.Y.: Paint selection. *ACM Transactions on Graphics (ToG)* **28** (2009) 69
32. Chen, Q., Li, D., Tang, C.K.: Knn matting. *IEEE transactions on pattern analysis and machine intelligence* **35** (2013) 2175–2188

## A Color Adjustment Operations

**Brightness** The brightness adjustment operation is defined as

$$\text{op}_b(x, \alpha_b) = \begin{cases} x \cdot (1 - \alpha_b) + \alpha_b, & \text{if } \alpha_b \geq 0 \\ x + x \cdot \alpha_b, & \text{otherwise} \end{cases} \quad (4)$$

where  $x$  is the input image, and  $\alpha_b$  is a scalar parameter that controls the extent of the adjustment. We clip  $\alpha_b$  into the range  $[-1, 1]$ .

**Saturation** The saturation adjustment operation is defined as

$$\text{op}_s(x, \alpha_s) = \begin{cases} x + (x - L(x)) \cdot s(x, \alpha_s), & \text{if } s > 0 \\ L(x) + (x - L(x)) \cdot (1 + s(x, \alpha_s)), & \text{otherwise} \end{cases} \quad (5)$$

where  $x$  is the input image, and  $\alpha_s$  is a scalar parameter that controls the extent of the adjustment. We clip  $\alpha_s$  into the range  $[-1, 1]$ .

$L(x)$  is the per-pixel average of the three channels  $\frac{1}{2} \cdot [\text{rgb\_max}(x) + \text{rgb\_min}(x)]$ , and  $s(x, \alpha_s)$  is defined as

$$s(x, \alpha_s) = \begin{cases} 1/S(x) - 1, & \text{if } \alpha_s + S(x) \geq 1 \\ 1/(1 - \alpha_s) - 1, & \text{otherwise} \end{cases}$$

$S(x)$  is defined as a per-pixel ratio

$$S(x) = \begin{cases} \text{delta}(x)/(2 \cdot L(x)), & \text{if } L < 0.5 \\ \text{delta}(x)/(2 - 2 \cdot L(x)), & \text{otherwise} \end{cases}$$

where  $\text{delta}(x) = \text{rgb\_max}(x) - \text{rgb\_min}(x)$ .

**Contrast** The contrast adjustment operation is defined as

$$\text{op}_c(x, \alpha_c) = \begin{cases} \bar{x} + (x - \bar{x})/(1 - \alpha_c), & \text{if } \alpha_c \geq 0 \\ \bar{x} + (x - \bar{x}) \cdot (1 + \alpha_c), & \text{otherwise} \end{cases} \quad (6)$$

where  $x$  is the input image,  $\bar{x}$  is the average of all pixel values of  $x$ , and  $\alpha_c$  is a scalar parameter that controls the extent of the adjustment. We clip  $\alpha_c$  into the range  $[-1, 1]$ .